Supplemental information

Sandra Ruiz-Gómez,[1,2] Lucas Pérez,[1,2] Arantzazu Mascaraque,[1,2] Adrian Quesada,[3] Pilar Prieto,[4] Irene Palacio,[5] Laura Martín-García,[6] Michael Foerster,[7] Lucía Aballe,[7] and Juan de la Figuera[6]

[1]*Dpto. de Física de Materiales, Universidad Complutense de Madrid, Madrid E-28040, Spain*
[2]*Unidad Asociada IQFR(CSIC)-UCM, Madrid E-28040, Spain*
[3]*Instituto de Cerámica y Vidrio, CSIC, Madrid E-28049, Spain*
[4]*Dpto. de Física Aplicada, Universidad Autónoma de Madrid, Madrid E-28049, Spain*
[5]*Instituto de Ciencia de Materiales de Madrid, CSIC, Madrid E-28049, Spain*
[6]*Instituto de Química Física "Rocasolano", CSIC, Madrid E-28006, Spain*
[7]*Alba Synchrotron Light Facility, CELLS, Barcelona E-08290, Spain*

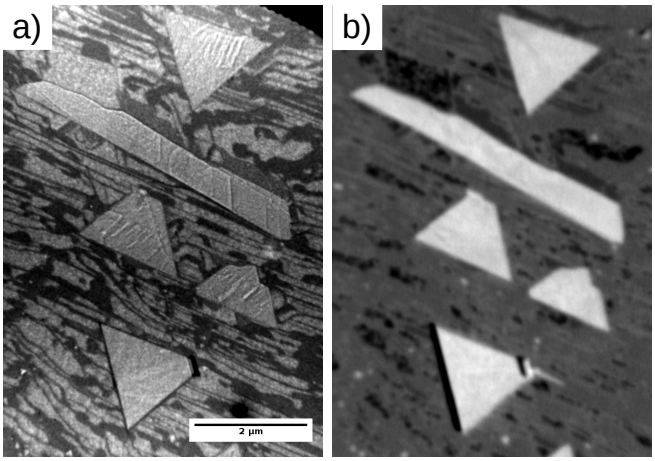

FIG. S1. (a) LEEM image of the five islands studied in the present work. (b) XAS image of the same area.

I. AREA WITH ALL THE ISLANDS PRESENTED IN THIS WORK

As indicated in the text, the islands whose magnetization maps have been studied in this work are all in the same vicinity, so the are expected to have a similar density of substrate steps. Their precise location is shown in Figure S1.

II. OBTAINING VECTOR MAGNETIZATION MAPS FROM MULTIPLE XMCD IMAGES

To obtain the spatially resolved vector magnetization vector on each island, three consecutive XMCD images are acquired at different azimuthal angles of the sample relative to the x-ray beam[1–3]. Each corresponds then to the component of the magnetization along the x-ray incidence direction. An example is shown in Figure S2. The three images in the top row (Figure S2a) have been acquired by first rotating the azimuth of the sample by 0, 60 and 120° respectively before each image acquisition. Then an opposite rotation is applied in software to get the same island orientation (Figure S2b). The images have distortions so they do not have the same shape. Then the second and third images are streched by an affine transformation so the island borders coincide with the first to correct for the image distortions (Figure S2c). The three images provide the magnetization component along three non-coplanar directions, taking into account that the polar angle of incidence of the beam is fixed at 74° relative to the sample normal. Considering the transformation from this skew reference system to an orthogonal one we obtain the components along x,y and z axis aligned with the horizontal, vertical and out of the image components (Figure S2d). From those, we obtain the azimuthal, polar and magnitude of the dichroic signal shown in the bottom row (Figure S2e).

III. XAS AND XMCD AND SUM RULES

We follow Chen et al.[4] to estimate the magnetic moments from the integrals of the XAS and XMCD spectra of L_3 and L_2. The XAS and XMCD spectra have been acquired integrating from an area within the upper domain in Figure 1. We integrate the XAS and XMCD spectra shown in Figure 1d and e, as shown in Figure S3. To obtain the integral of the XAS spectra, an hyperbolic tangent background is subtracted to remove the step of each absorption edge. The background $tanh$ center is positioned at the middle of each absorption edge, and the height to the height after the edge. No correction has been done for the magnetic dipolar operator. Then the integrals of the XAS spectrum (Figure S3b) after both absorption edges (r), and of the XMCD spectrum after the L3 (p) and L2 (q) absorption edges are measured as indicated in the plot. The orbital and spin moment of magnetite are estimated assuming a number of holes N_h=13.5 and following the sum rules[4]:

$$m_{spin} = -\frac{(6p-4q)}{r} N_h \quad (1)$$

$$m_{orbital} = \frac{4q}{3r} N_h \quad (2)$$

IV. MICROMAGNETIC CALCULATIONS

The shape of each island was extracted from the experimental images and used to define the material region in the micromagnetic simulation. Then the dichroic vector signal, proportional to the local magnetization, was used as the initial

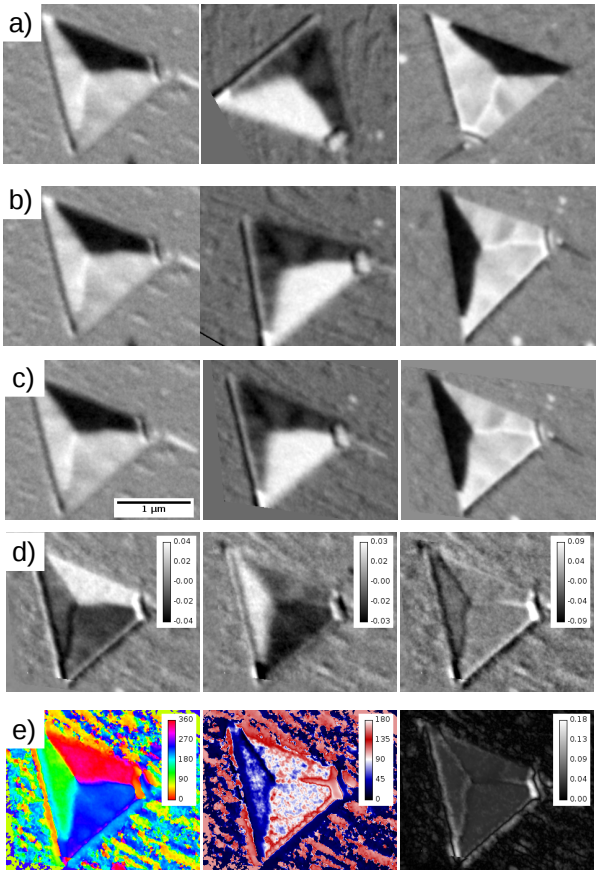

FIG. S2. Sequence of steps to obtain the map of the magnetization vector from XMCD images. For explanation, see text. (a) Original XMCD images acquired at an azimuthal angle of 0, 60 and 120°. (b) Images rotated back, so each image corresponds to the x-ray rotated by 0, 60 and 120°. (c) Corrected XMCD images after the application of an affine transformation relative to the first island. (d) Components of the dichroic signal along the x, y and z directions in the figures where x,y and z correspond to the horizonal, vertical and out-of-page axis of the figure. (e) Same dichroic vector in spherical coordinates. Each image corresponds (from left to right) to the azimuthal angle, the polar angle, and the magnitude.

configuration of a micromagnetic simulation. Then the material parameters were changed and the configuration was relaxed again with the new parameters. Finally the domain wall width in the simulation was measured by estimating the jump from 20% to 80% of the x-component of the magnetization after removing a constant slope.

V. GENERAL OVERVIEW OF THE IMAGES BEFORE AND AFTER ANNEALING

In Figure S4 we show the area with the islands studied in the present work, as-grown and after the annealing step.

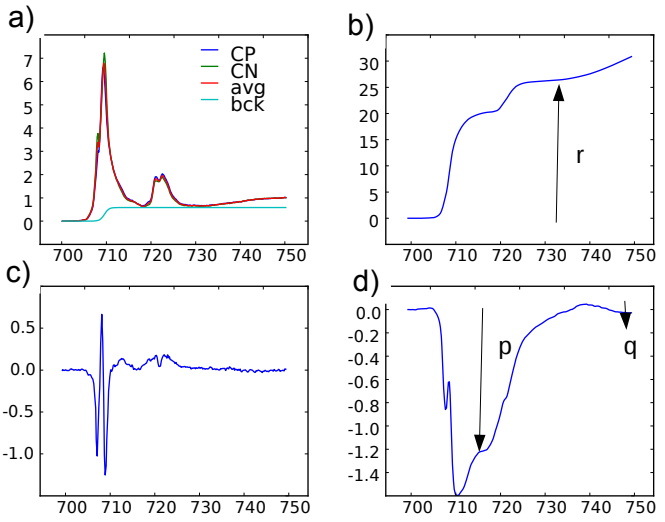

FIG. S3. XAS and XMCD spectra used to estimate the magnetic moment of iron. a) XAS spectra, including the spectrum with both helicities, the averaged spectra and the hiperbolic tangent background. b) Integral of the averaged XAS spectra. c) XMCD spectra. d) integral of the XMCD spectra.

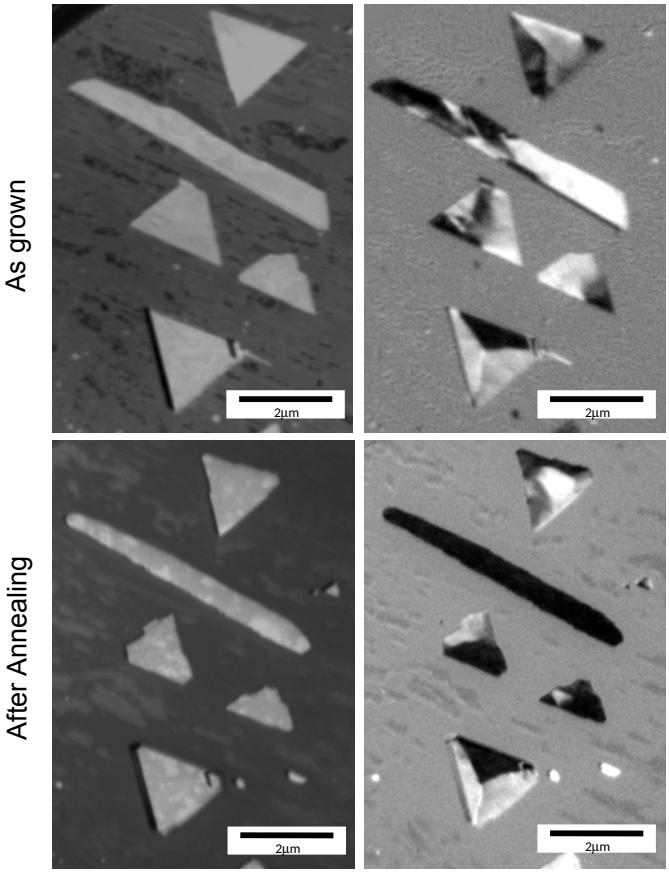

FIG. S4. Top: XAS and XMCD image of the five islands, as-grown, studied in the present work. Bottom: XAS and XMCD image of the same area after annealing the film as described in the main text.

ACKNOWLEDGMENTS

This work is supported by the Spanish Ministry of Economy and Competitiveness through Projects No. MAT2015-64110-C2-1-P, MAT2015-64110-C2-2-P, MAT2014-52477-C5-2-P and MAT2013-48009-C4-1-P and by the European Comission through Project H2020 No. 720853 (Amphibian). These experiments were performed at the CIRCE beamline of the ALBA Synchrotron Light Facility. I.P. acknowledges the EU via the innovation program under grant agreement No. 696656 (GrapheneCore1-Graphene-based disruptive technologies).

[1] L. Le Guyader, A. Kleibert, A. Fraile Rodríguez, S. El Moussaoui, A. Balan, M. Buzzi, J. Raabe, and F. Nolting, "Studying nanomagnets and magnetic heterostructures with X-ray PEEM at the Swiss Light Source," J. Elec. Spec. Photoelectron microscopy, Time resolved pump-probe PES, **185**, 371–380 (2012).

[2] X. Moya, L. E. Hueso, F. Maccherozzi, A. I. Tovstolytkin, D. I. Podyalovskii, C. Ducati, L. C. Phillips, M. Ghidini, O. Hovorka, A. Berger, M. E. Vickers, E. Defay, S. S. Dhesi, and N. D. Mathur, "Giant and reversible extrinsic magnetocaloric effects in $La_{0.7}Ca_{0.3}MnO_3$ films due to strain," Nat. Mater. **12**, 52–58 (2013).

[3] J. de la Figuera, "How to obtain XMCD-PEEM vector maps," `http://surfmoss.iqfr.csic.es/xmcd` (2017), accessed: 2017-09-23.

[4] C. T. Chen, Y. U. Idzerda, H.-J. Lin, N. V. Smith, G. Meigs, E. Chaban, G. H. Ho, E. Pellegrin, and F. Sette, "Experimental confirmation of the x-ray magnetic circular dichroism sum rules for iron and cobalt," Phys. Rev. Lett. **75**, 152–155 (1995).